RESEARCH ARTICLE

A Parsimonious Model of the Rabbit Action Potential Elucidates the Minimal Physiological Requirements for Alternans and Spiral Wave Breakup

Richard A. Gray*, Pras Pathmanathan

Division of Biomedical Physics, Office of Science and Engineering Laboratories, Center for Devices and Radiological Health, Food and Drug Administration, Silver Spring, Maryland, United States of America

* Richard.Gray@fda.hhs.gov

Abstract

Elucidating the underlying mechanisms of fatal cardiac arrhythmias requires a tight integration of electrophysiological experiments, models, and theory. Existing models of transmembrane action potential (AP) are complex (resulting in over parameterization) and varied (leading to dissimilar predictions). Thus, simpler models are needed to elucidate the "minimal physiological requirements" to reproduce significant observable phenomena using as few parameters as possible. Moreover, models have been derived from experimental studies from a variety of species under a range of environmental conditions (for example, all existing rabbit AP models incorporate a formulation of the rapid sodium current, I_{Na}, based on 30 year old data from chick embryo cell aggregates). Here we develop a simple "parsimonious" rabbit AP model that is mathematically identifiable (i.e., not over parameterized) by combining a novel Hodgkin-Huxley formulation of I_{Na} with a phenomenological model of repolarization similar to the voltage dependent, time-independent rectifying outward potassium current (I_K). The model was calibrated using the following experimental data sets measured from the same species (rabbit) under physiological conditions: dynamic current-voltage (I-V) relationships during the AP upstroke; rapid recovery of AP excitability during the relative refractory period; and steady-state I_{Na} inactivation via voltage clamp. Simulations reproduced several important "emergent" phenomena including cellular alternans at rates > 250 bpm as observed in rabbit myocytes, reentrant spiral waves as observed on the surface of the rabbit heart, and spiral wave breakup. Model variants were studied which elucidated the minimal requirements for alternans and spiral wave break up, namely the kinetics of I_{Na} inactivation and the non-linear rectification of I_K. The simplicity of the model, and the fact that its parameters have physiological meaning, make it ideal for engendering generalizable mechanistic insight and should provide a solid "building-block" to generate more detailed ionic models to represent complex rabbit electrophysiology.

Author Summary

Understanding and preventing life-threatening irregular electrical heart rhythms includes basic experimental, numerical, and theoretical research. Computer models of the electrical dynamics of cardiac cells and impulse propagation throughout the heart are essential tools of this research. For example, simulations of electrical activity such as rotating 'spiral waves' have been used to understand how irregular heart rhythms are maintained. However, existing models are derived exclusively from sub-cellular data under a variety of environmental conditions and species. These models tend to be exceedingly complex including hundreds of variables and parameters which make them difficult to validate and analyze. Using experimental data from one species (rabbit) under nearly identical physiological conditions, we developed a simple model of the electrical activity of a cardiac cell derived from sub-cellular, cellular, and tissue experimental data. This model reproduces cellular excitability and its recovery as well as several important "emergent" phenomena including beat-to-beat cellular alterations and unstable spiral waves. Under some conditions, unstable spiral waves in this model give rise to continuous formation of new spiral waves (i.e., "spiral wave breakup") which is thought to be the underlying cause of cardiac fibrillation and sudden cardiac death.

Introduction

The simulation of action potentials (APs) and their propagation has been an integral part of the field of electrophysiology for over half a century.[1] Over a hundred cellular AP models from many regions of the heart encompassing a variety of species have been published. These "ionic" models have been derived almost exclusively from voltage clamp data from a variety of species, often recorded under conditions that are not physiological. Ionic models are increasingly complex, and are comprised of numerous sub-models (mostly transmembrane currents), and contain tens of variables and hundreds of parameters. For example, a recent meta-analysis found that 50% of the data used in the development of the ten-Tusscher-Panfilov [2] and Iyer [3] human ventricular models were of non-human origin [4]. While their complexity has many advantages, there are a variety of limitations including: over-parametrization[5]; non-uniqueness/multi-stability [6, 7]; dissimilar predictions [8–12]; limited validation outside their development domain [13] (e.g. using a cell model derived from voltage clamp data to study reentrant arrhythmias); difficulty in representing natural "physiological redundancy" (e.g. repolarization reserve [14]); interpreting the relative roles of model sub-components on model predictions; and generalizing insight from "model-specific" simulations results.

An alternative, and complementary approach compared to these ionic models, is to use "phenomenological" models which are designed to represent specific, often macroscopic phenomena (e.g., rate dependence of action potential duration)[15–19]. Phenomenological models are designed to reproduce one (or two) specific phenomena(on) very well, and are: simplistic, computationally efficient, and sometimes amenable to analytical approaches. However, unlike ionic models, phenomenological models do not provide a direct link to physiologically meaningful model parameters derived experimentally. Therefore phenomenological models provide only limited mechanistic insight, and are not amenable for reproducing numerous phenomena, nor can they be easily extended.

The two most important membrane currents for cardiac excitability are the rapid sodium current (I_{Na}) and the rectifying potassium current (I_{K1}), which are both highly non-linear functions of transmembrane potential (V_m). I_{Na} is responsible for the rapid all-or-none

depolarization of the AP upstroke, and I_{K1} is responsible for maintaining the resting potential near -85 mV. In fact, it has been shown recently that transfecting cells with genes encoding for cardiac I_{Na}, I_{K1}, and gap junctions Cx43 (only) into unexcitable somatic cells can transform monolayers into excitable tissue capable of supporting propagating "cardiac" action potentials including reentrant "spiral" waves![20]

Due to the ethical and practical limitations involved in studying human physiology, animal experiments are necessary to understand and develop clinical strategies aimed at treating the pathological mechanisms underlying heart disease. The isolated rabbit heart has been shown to share certain electrophysiological characteristics as the human, including repolarization reserve [21] and ventricular fibrillation dynamics.[22] as well as the effects of many pharmaceuticals. [23]

All existing ionic models of the rabbit ventricular AP [24–27] incorporate the I_{Na} equations from the LR1 guinea pig model,[28] albeit with different conductance values. The LR1 I_{Na} equations incorporate the gating kinetics of fast activation, fast inactivation and slow inactivation. The fast activation and fast inactivation equations were derived from voltage clamp (VC) data from spherical clusters of eleven day-old embryonic chick heart cells,[29] and slow inactivation parameters were based on VC results from sheep and pig ventricular trabeculae.[30] Obviously, there is a need to update rabbit AP models to incorporate an I_{Na} model based on rabbit data, but this is not a simple task. To date, I_{Na} activation parameters have been derived exclusively from VC protocols; however, since the I_{Na} current in the adult myocyte is too large to allow adequate voltage control under physiological conditions,[31] these VC protocols are carried out at low temperatures with low extracellular sodium concentrations or in HEK cells or oocytes transfected with the SCN5A gene which encodes the cardiac I_{Na} channel (Na_v 1.5).

The first aim of this paper is to develop a "parsimonious" model for the rabbit myocyte AP based *only* on data recorded from the rabbit under physiological conditions. A model is considered parsimonious if it accomplishes a desired level of explanation or prediction with as few parameters as possible (although, as far as we are aware, there is no definitive and scientifically rigorous definition of parsimonious). For this paper, the desired level of prediction is the following well-known and important electro-physiological phenomena, measured from rabbit ventricular myocytes/tissue under nearly identical and physiological conditions: 1) steady-state inactivation as determined from voltage clamp experiments [31]; 2) action potential depolarization in single cells; 3) recovery of AP excitability in single cells[32]; and 4) action potential depolarization dynamics during propagation in the whole heart. [33] For calibration and evaluation of the model we coupled this I_{Na} model with various models of I_{K1}, and also explored a range of cellular and tissue behavior in an AP model incorporating a previously published phenomenological two parameter model of repolarization.[33] The overall model will be referred to as the parsimonious rabbit (PR) model. The second aim of this paper is to demonstrate that this simple and parsimonious model is sufficient for reproducing important "emergent" complex phenomena such as alternans and spiral wave breakup, which suggests a novel physiological mechanism for arrhythmia instabilities.

Methods

Parsimonious Rabbit (PR) I_{Na} Sub-model Formulization

The equations of I_{Na} are of the form pioneered by Hodgkin-Huxley (HH) [1]

$$I_{Na} = g_{Na} m^3 h (V_m - E_{Na}),\tag{1}$$

where V_m is the transmembrane potential, g_{Na} is the maximal conductance of I_{Na}, m (fast activation), and h (fast inactivation) are gating variables, and E_{Na} is the Nernst equilibrium

potential for sodium. Beeler and Reuter [34] introduced a slow inactivation gate (j)

$$I_{Na} = g_{Na}m^3 hj(V_m - E_{Na}),$$

(2)

which has been incorporated into all of the most recent cardiac HH I_{Na} models.[24–27].

The HH equations for the gating variables are of the form:

$$\frac{dy}{dt} = \alpha_y(1-y) - \beta_y y \equiv \frac{y_\infty - y}{\tau_y},$$

(3)

where y represents each gating variable, $\alpha_y(V_m)$ and $\beta_y(V_m)$ represent the on and off rate constants for gating (respectively) which are voltage dependent, $y_\infty(V_m)$ and $\tau_y(V_m)$ are the steady state fraction of activation or inactivation and time constant (respectively) and are functions of V_m. Hodgkin and Huxley [1] fit their voltage clamp data to empirically determine the functions $\alpha_y(V_m)$ and $\beta_y(V_m)$ using only 9 parameters; in contrast the LR1 I_{Na} equations contain 31 parameters. Since 1952 there has been significant advancement in the derivation of gating equations based on first principles.[35, 36] The simplest functional form for the rate equations of voltage dependent gating based on thermodynamics and chemical reaction rates are:[37]

$$\alpha_y = \alpha_y^0 \exp\left(\frac{-\delta_y V_m}{k_y}\right) \quad , \quad \beta_y = \beta_y^0 \exp\left(\frac{(1-\delta_y)V_m}{k_y}\right),$$

(4)

where the constants α_y^0, β_y^0, and $0 \le \delta_y \le 1$ are positive, while $k_y < 0$ for activation and $k_y > 0$ for inactivation. Using Eq 3 we can derive the equations for $y_\infty(V_m)$ and $\tau_y(V_m)$ from Eq 4:

$$y_\infty(V_m) = \frac{1}{1 + \exp\left[\frac{(V_m - E_y)}{k_y}\right]},$$

(5)

and

$$\tau_y(V_m) = \frac{2\tau_y^0 \exp\left[\frac{\delta_y(V_m - E_y)}{k_y}\right]}{1 + \exp\left[\frac{(V_m - E_y)}{k_y}\right]}.$$

(6)

There are 4 parameters per gate ($E_y, k_y, \tau_y^0, \delta_y$) in this formulization. The main limitation of this formulization is that $\tau_m(V_m) \rightarrow 0$ away from E_m which is not realistic, because gating transformations cannot be instantaneous. For example, the LR1 equations predict $\tau_m(-85mV) = 0.0055\ ms$ and $\tau_m(+30mV) = 0.041\ ms$ at 37 C, however these values are below the resolution of voltage clamp measurements. We address this problem by removing the V_m dependence of τ_m (making it a constant, thus eliminating parameter δ_m). To summarize, we define the novel PR I_{Na} submodel using Eqs 1 and 3, with m_∞ and h_∞ given by Eq 5, τ_h given by Eq 6, and τ_m equal to a constant.

Parsimonious Rabbit (PR) I_{Na} Sub-model Calibration

All model parameters are provided in **Table 1**. Values for E_h and k_h where taken directly from Table 1 in [31]. We set $E_{Na} = 65mV$, and all other parameters were determined via manual fitting to the experimental data described below using no more than 2 significant digits; τ_h^{max} and δ_h were computed via "inverting" Eq 6 given the two value pairs $\tau_h(-80mV) = 4.0ms$ and $\tau_h(0mV) = 0.45ms$.

Simulations required for the calibration were carried out in single cells and a one-dimensional cable by integrating the three ordinary differential equations using exact integration for

Table 1. Parameter values for "parsimonious rabbit" (PR) model.

current	parameter	value	units
I_{Na}	g_{Na}	11	mS/µF
	E_m	-41	mV
	k_m	-4.0	mV
	τ_m	0.12	ms
	E_h	-74.9	mV
	k_h	4.4	mV
	τ_h^0	6.80738	ms
	δ_h	0.799163	none
I_K	g_K	0.3	mS/µF
	b	0.047	mV^{-1}

doi:10.1371/journal.pcbi.1005087.t001

the gating variables and forward Euler integration for V_m with dt = 0.001 ms which is actually a very conservative choice made because of the low computational cost. The fact that τ_m is constant provides for a well-defined minimum time constant of the model which allows for the use of larger values of dt and computational efficiency compared to other models. [38] Cable simulations were performed using a central difference approximation of the Laplacian in a 4 cm long cable using $I_{ion} = I_{Na} + I_{K1L}$ (in order to establish a steady-state resting membrane potential) with diffusion coefficient (D) equal to 0.001 cm^2/ms and dx = 0.01 cm, where I_{K1L} is the formulation of I_{K1} provided by Livshitz and Rudy [39]. I_{Na} and V_m signals were recorded at the center of the cable to construct the I-V curves for calibration to the experimental data as described below.

Dynamic Current-Voltage Relationship during the Action Potential Upstroke

The current during the AP upstroke is predominately I_{Na}, therefore the precise time course of $V_m(t)$ contains a wealth of information regarding I_{Na} kinetics.[40–42] In isolated myocytes the time course of I_{Na} can be estimated as $I_{ion} = -C_m \frac{dV_m}{dt}$ (after the stimulus current is turned off), where C_m is the specific membrane capacitance which we assume is equal to 1 µF/cm^2. During propagation, however, the total transmembrane current is *not* proportional to $\frac{dV_m}{dt}$; but we recently developed a methodology and justified the computation of I_{Na} as $C_m \left(\frac{D}{(CV)^2} \frac{d^2V_m}{dt^2} - \frac{dV_m}{dt} \right)$ during the AP upstroke during planar wave propagation, where CV is the conduction velocity [33]. These relationships were used to calibrate our model to dynamic I-V curves from glass microelectrode V_m measurements during AP upstrokes from isolated rabbit ventricular myocytes[43] and from the epicardial surface during planar propagation on the surface of the isolated Langendorrff-perfused heart.[33] In isolated myocytes V_m traces from APs stimulated with near threshold stimuli with a latency of 2.5 ms (range of 1.2 to 3.7 ms) were chosen from a previous study[43], because this latency provided datum during the early decrease I_{Na} of near –40 mV. Similar to Joyner et al. [32] we found a slight decrease (5.2 ± 0.5 mV/ms per ms) of $\left(\frac{dV_m}{dt} \right)_{max}$ as a function of latency which corresponds to only a 3.4% decrease compared to the traditional latency value of 1 ms.

Recovery of Action Potential Excitability Protocol

It is well known that $\left(\frac{dV_m}{dt} \right)_{max}$ is decreased during the relative refractory period of the AP, and this is thought to be a *cellular* phenomenon [32]. Here we assume that this phenomena

("recovery of AP excitability") is controlled only by the voltage and time dependent I_{Na} current and the AP shape. To reproduce the experimental results of recovery of AP excitability in isolated myocytes,[32] we developed a novel "virtual protocol". This protocol involves simulating an action potential clamp of I_{Na} using APs measured during pacing from six isolated myocytes recorded in a previous study.[43] During the 11th beat the simulations were switched to current-clamp mode and stimulated with a 2 ms stimulus at various coupling intervals; the amplitude was adjusted such that the latency was 1 ms. The resulting peak I_{Na} was normalized to that recorded during the 10th beat and presented as a function of coupling interval.

Comparison with Previous Models

Since the I_{Na} equations in all previous rabbit models are identical to LR1, except for scaling (conductances), we present previous model predictions using LR1 with two conductance values (23 mS/μF and 8 mS/μF) to cover the entire range (grey lines in figures). In addition we present results from the Ebihara-Johnson (EJ) model [29] (dashed grey lines) which is identical to LR1, except it does not contain slow inactivation.

Parsimonious Rabbit (PR) Cell Model

To create our parsimonious rabbit (PR) cell model, we combined our model of I_{Na} with a previously published phenomenological model of repolarization (I_K) designed to reproduce rabbit AP repolarization during propagation:

$$I_K = g_K e^{-b(V_m - E_K)}(V_m - E_K),$$
(7)

where g_K is the maximal conductance of I_K, b is a parameter controlling AP shape, and E_K is the reversal potential for potassium (set equal to the average resting potential of the six cells in **Fig 1** of -83 mV); the nominal parameters values for I_K are provided in **Table 1**, as previously determined.[33] We define our PR cell model via a total ionic current of $I_{Na} + I_K$ in Eqs 1 and 5–7 with parameters in **Table 1**.

Results

Dynamic Current-Voltage Relationship during the Action Potential Upstroke

The experimental traces of V_m during AP depolarization of isolated rabbit ventricular myocytes are shown in **Fig 1A**; the traces are aligned to $\left(\frac{dV_m}{dt}\right)_{max}$. The average dynamic I-V curve during the AP upstroke for these traces are plotted as symbols (● representing the mean ± standard error of the mean) in **Fig 1B**. The calibrated PR results are shown as a thick black line. Previous model predictions (grey lines) bracket the range of peak I_{Na} but do not accurately capture the initial inward current deflection of the experimental I-V relationship (see box).

The experimental dynamic I-V curves during the AP upstroke during *propagation* from [33] are shown as symbols (●) in **Fig 2A**. Similar to above, previous model predictions (grey lines) span the range of peak I_{Na} but do not accurately capture the initial inward current deflection of the experimental I-V curve (see box). Although the PR model fits the initial decrease of I_{Na} and maximum V_m well, it does not match the experimental dynamic I-V curve during the second half of the upstroke.

It is important to note that the experimental dynamic I-V curves for isolated myocytes (Fig 1B) is different than that obtained during propagation (Fig 2A). To quantify these differences we fit both curves to fifth order polynomials and identified the regions in which the 95% confidence intervals of these fits did not overlap (see Fig A in S1 Text). The inward current during
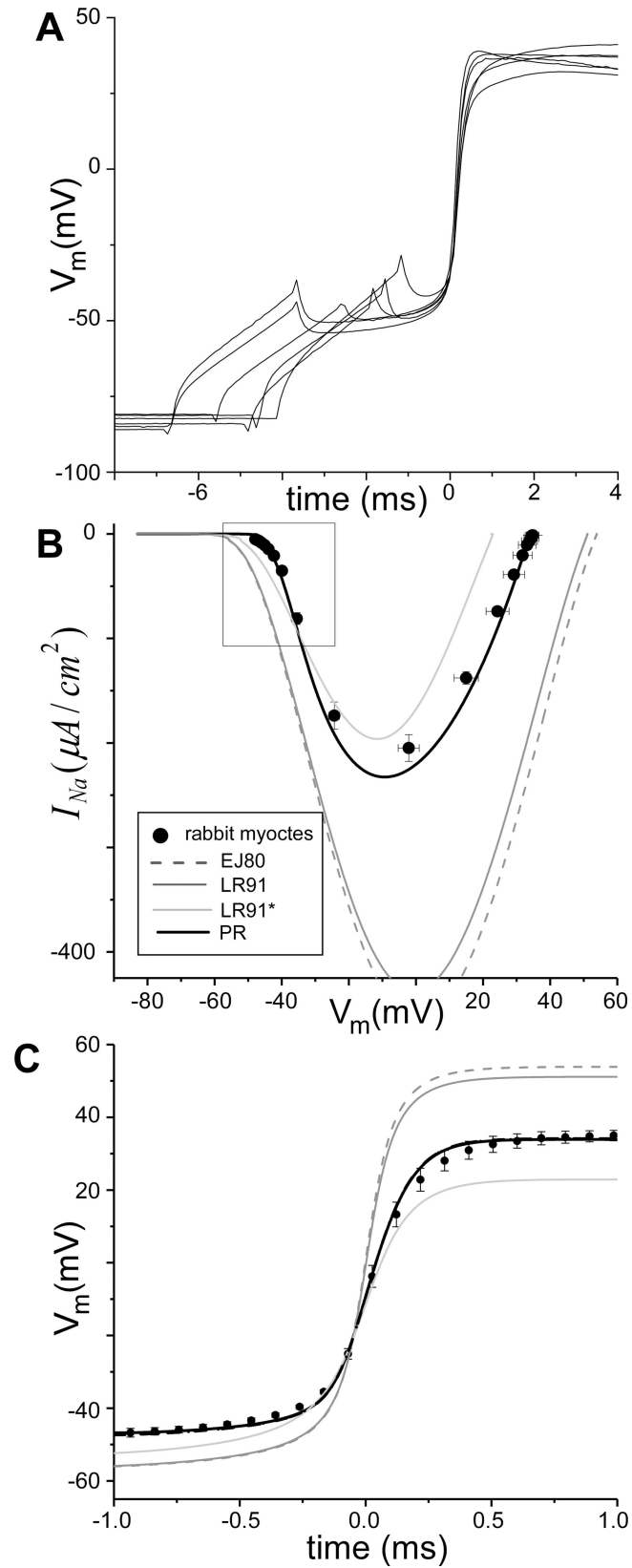
Fig 1. Dynamic I-V curves from isolated cells. A) Transmembrane potential (V_m) recorded during the action potential upstroke from six isolated rabbit cells from [43]. B) Current-voltage (I-V) relationship plotted as I_{Na} (models: lines) or $-C_m \frac{dV_m}{dt}$ (experiments: ●) versus V_m. C) Predicted V_m signals from models (lines) and average from experiments (●) during the upstroke.

the upstroke for myocytes was more negative compared to during propagation for -41 mV < V_m < -22 mV and for V_m > +4.5 mV.

Recovery of Cellular Excitability

The normalized magnitude of peak I_{Na} as a function of recovery time are shown in **Fig 3B**; experimental results from [32] are shown as symbols (●), PR model results are shown as a thick black line, and previous model predictions shown in grey. Simulation results (i.e., lines) include standard error bars because the virtual protocol includes six different APs and thus include the effect of normal variation of AP shape. *Unlike previous models with slow inactivation (Eq 2), the PR and EJ80 models which include only fast inactivation (Eq 1) are consistent with the experiments.*

Steady State Activation, Inactivation, and Time Constants

The voltage dependence of steady state I_{Na} activation and inactivation as well as the corresponding time constants are shown in **Fig 4** for our PR model, as well as LR1, and EJ models. Our PR model exhibits a steeper activation slope at slightly less depolarized voltages compared to LR1 and EJ (panel A). As described above, τ_m in the PR model does *not* exhibit voltage dependence but is similar to the mean value of LR1 and EJ (panel B). The steady state I_{Na} inactivation for PR is more negative compared to LR1 and EJ (panel C) and the maximum value of τ_h for PR is less than that for τ_h for LR1 and EJ80 and is considerably less than τ_j for LR1 (panel D).

Robustness of PR I_{Na} Sub-model

The PR results in **Figs 1 and 2** represent the results from for our novel I_{Na} *sub-model only*; the results in **Fig 3** include coupling to the I_{K1L} sub-model. To assess the effect of repolarization current on the PR results shown in **Figs 1–3** we reran all simulations with cell models incorporating I_{K1L} or the phenomenological model of repolarization Eq 7 (PR cell model). The results from these simulations were nearly identical to the PR I_{Na} sub-model *only*; in fact the results are shown as thick dashed (I_{K1L}) and dotted (I_K) lines in **Figs 1–3** but cannot be seen because they superimpose upon the solid black line.

Simulations using our PR cell model resulted in APs with the following characteristics: $I_{Na}^{min} = -233 \mu A/cm^2$, $V_m^{max} = 34\, mV$ and $APD = 197 ms$ for single cells; and $I_{Na}^{min} = -289 \mu A/cm^2$, $V_m^{max} = 24\, mV$, $CV = 55\, cm/s$ and $APD = 142 ms$ for propagation in a cable. With the exception of APD, these values were not significantly altered ($< 2\%$) compared to simulations using I_{K1L} [39] or I_K [33] indicating that the predictions of our PR I_{Na} sub-model are quite insensitive to the specific choice of repolarization current.

We performed parameter sensitivity analysis by quantifying the effect of a 1% variation of the eight I_{Na} gating parameters on eight quantities of interest; results are provided in the Table A in S1 Text as an 8x8 matrix. We also characterized the effect of AP shape on cell and tissue-level behavior for our new PR model ($I_{Na} + I_K$) by varying repolarization parameters g_K and b over the entire "physiological range" for all mammals: reported values of g_K range from 0.1 to 0.5 mS/μF and the range of b values chosen, $0.03 \leq b \leq 0.05$ mV^{-1}, correspond to APDs ranging from 23 ms to 516 ms. The results are displayed in the Figs B and C in S1 Text. Over this range of g_K and b, I_{Na}^{min} varied 1.6% and V_m^{max} varied 1.2% in single cells, while during
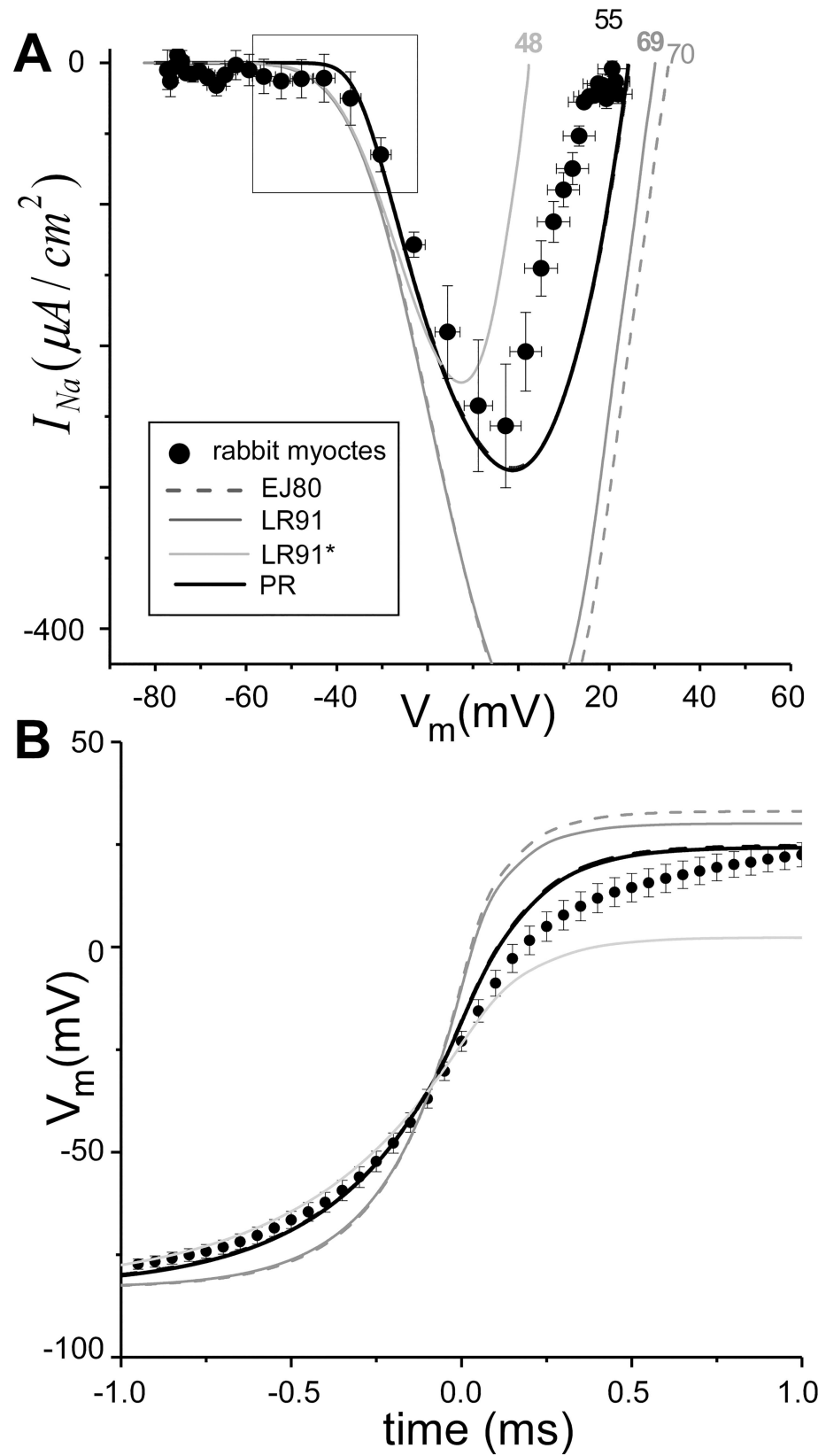
Fig 2. Dynamic I-V relationship during propagation. A) Current-voltage (I-V) relationship plotted as I_{Na} (models) or I_{ion} (experiments: ● from [33]) versus V_m. Values of CV for each model are shown at the top. B) Predicted transmembrane potential (V_m) for the action potential upstroke during propagation for the models (lines) and average from experiments (●).

propagation the following quantities exhibited a fairly small dependence on I_K parameters: $I_{Na}^{\min}$: 1.8%; $V_m^{\max}$: 7.5%; CV: 4.5%. *The fact that action potential depolarization characteristics are fairly insensitive to repolarization in single cells and during propagation provides support for the robustness of our I_{Na} model.*

Model Evaluation

To confirm that the data used in the model calibration is representative, we compared several model results to experimental data from previously published studies. Table B in S1 Text demonstrates that the following model results are within the range found in the literature: resting membrane potential, action potential amplitude, $(dV_m/dt)_{\max}$, and CV.

In addition, we compared the predictions of spiral waves in the PR and Mahajan (M08) models (5 cm x 5 cm) to those recorded in the whole rabbit heart by Schalij et al.[44] Schalij et al found that only fibrillation was observed in the intact heart but that, after freezing the inside of the heart, stable reentry occurred around a linear line of conduction block of ~ 2 cm with a cycle length of 130 ± 11 ms.[44] Simulation results for PR and M08 are shown in **Fig 5**. The cycle length (~ 150 ms) and line of block (~ 3.2 cm) for PR using the nominal parameter values were larger than the experiments. Incidentally, decreasing parameter *b* by only 4% decrease improved the correspondence considerably (cycle length: ~125 ms; line of block: 2.5 cm as shown in the middle, right panel of **Fig 6** below). This change is justified because the PR model does not include any repolarization kinetics and is not developed to reproduce APD shortening with rate. In contrast to the experimental results of Schalij et al., [44] the line of block in our simulations was not static, but rotated which is typical of spiral wave simulations.[2] Simulations with M08 resulted in non-sustained unstable reentry with average cycle length of length (~ 150 ms); the tip trajectory traversed the majority of the region, and eventually terminated by hitting the top boundary. There was evidence of wave break (see green and blue trajectories in **Fig 5B** consistent with previous results indicating SWB for this model in a 7.5 cm x 7.5 cm region.

The level of validation required for a model depends on its "context of use" and the consequences of incorrect model predictions[13]. Hence further validation is expected to be required for each specific context. The preliminary validation performed here is appropriate for using the model to gain insight into underlying physiological mechanisms as demonstrated below.

Spiral Wave Dynamics

During "functional" spiral wave reentry the depolarization and repolarization processes are *inter*dependent. As shown in **Fig 6**, the dynamics of spiral waves in our model varied considerably as a function of repolarization (i.e., g_K and *b*). Spiral waves were not stable (i.e., rotationally symmetric) for any parameter pairs (g_K, *b*) in the range studied. For 8 of 9 parameter pairs, the spiral wave tip followed typical non-circular trajectories, while spiral wave breakup (SWB) occurred for one parameter set ($g_K = 0.5$, $b = 0.035$). The frequency of activity for single spiral waves ranged from ~3 Hz to ~18 Hz and the frequency of activity during SWB was ~30 Hz.

Alternans

Since SWB was observed (albeit for parameters corresponding to $APD = 23ms$ which is *not* consistent with normal rabbit physiology) we investigated whether cellular alternans occurred
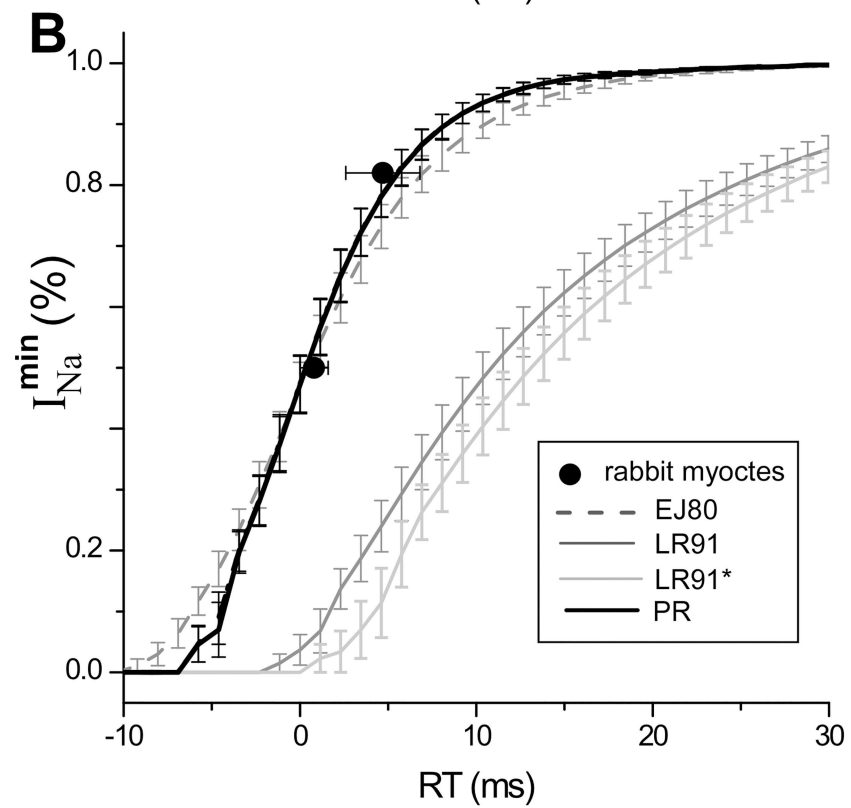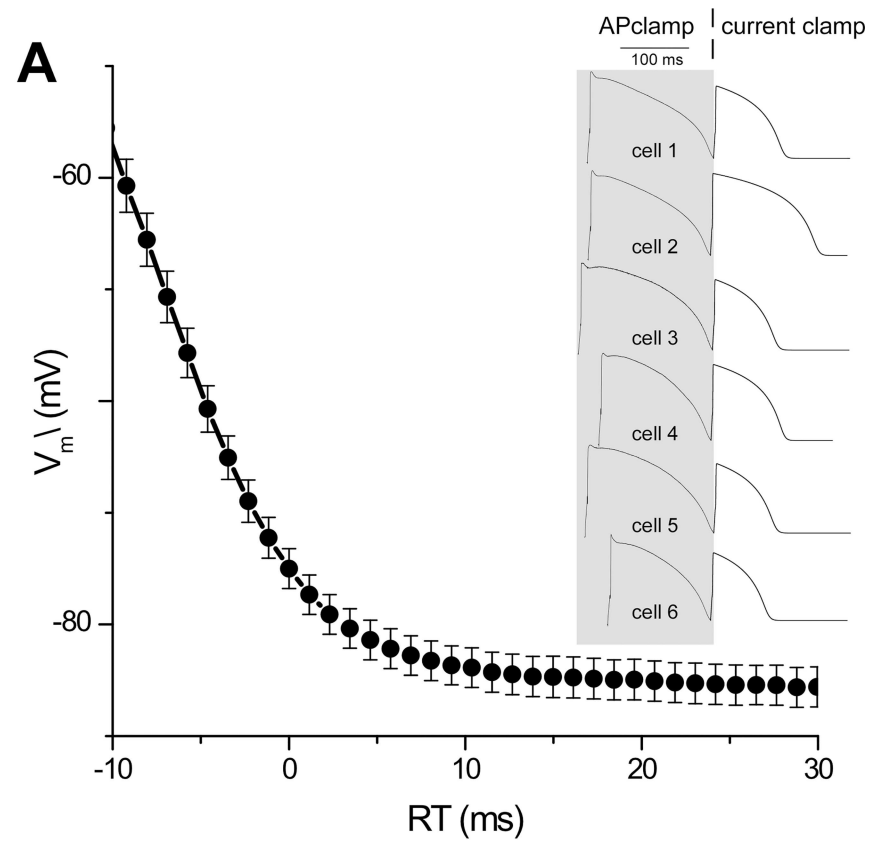
Fig 3. Recovery of AP excitability virtual protocol. A) Average V_m (●) of six experimental cells shown in inset, aligned to recovery time (RT: defined as the time at which V_m recovers to within 5 mV of the resting potential). B) Normalized peak I_{Na} (models: lines) or $\left(\frac{dV_m}{dt}\right)_{max}$ (experiments: ●) as a function of RT. Experimental values of RT at 50% (0.8 ± 0.8 ms) and at 82% (4.7 ± 0.8 ms) were taken from in Table 1 of [32]. The error bars in B) reflect the variability of AP shape of the six cells (see panel A). The novel action potential clamp virtual protocol is described in the text.

doi:10.1371/journal.pcbi.1005087.g003
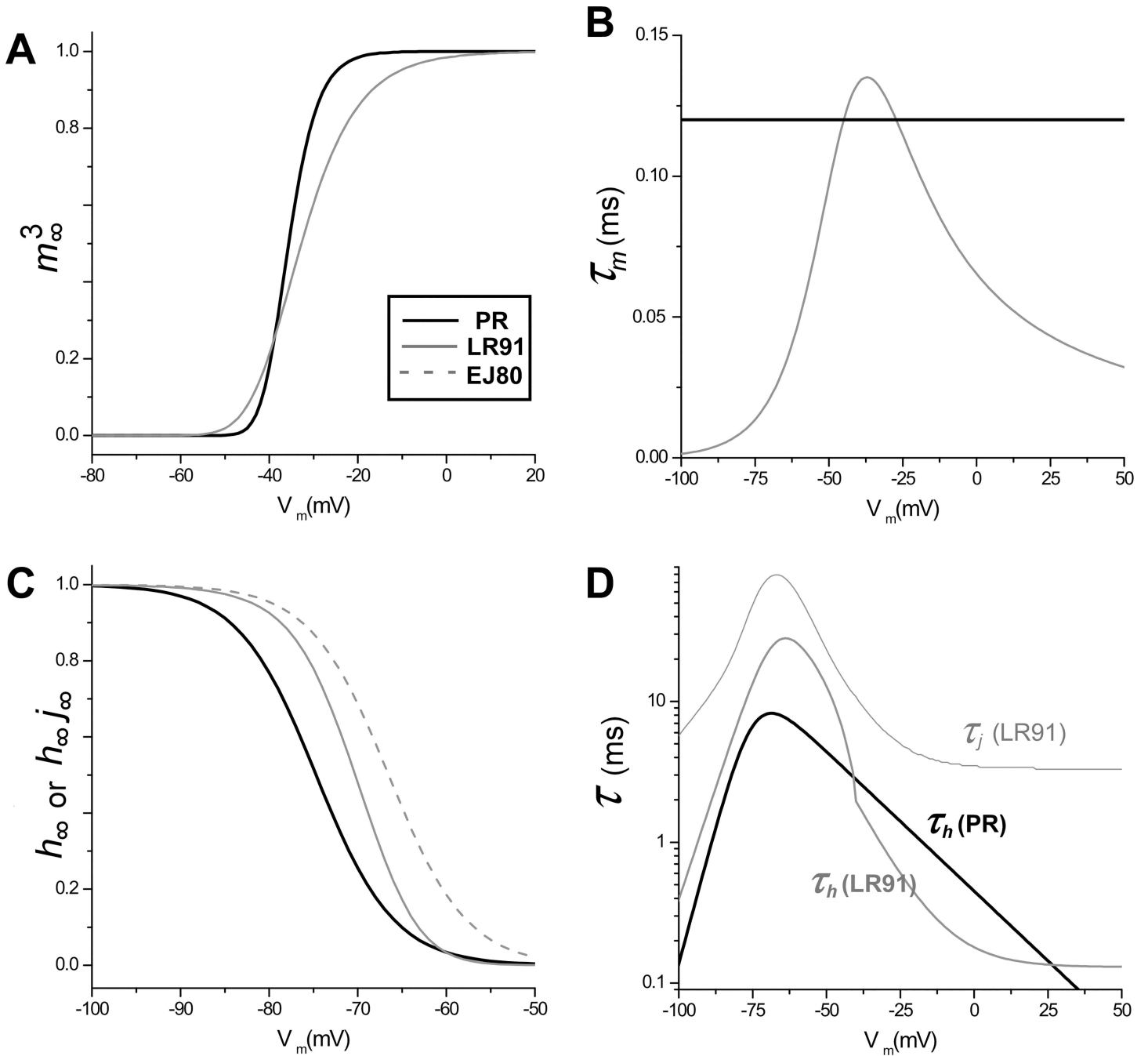
Fig 4. Voltage dependence of steady state I_{Na} activation (A), time constant for activation (B), steady state I_{Na} inactivation (C), and time constant for inactivation (D) for the PR (black), LR1 (grey), and EJ (dashed grey) models (note the log scale).

doi:10.1371/journal.pcbi.1005087.g004
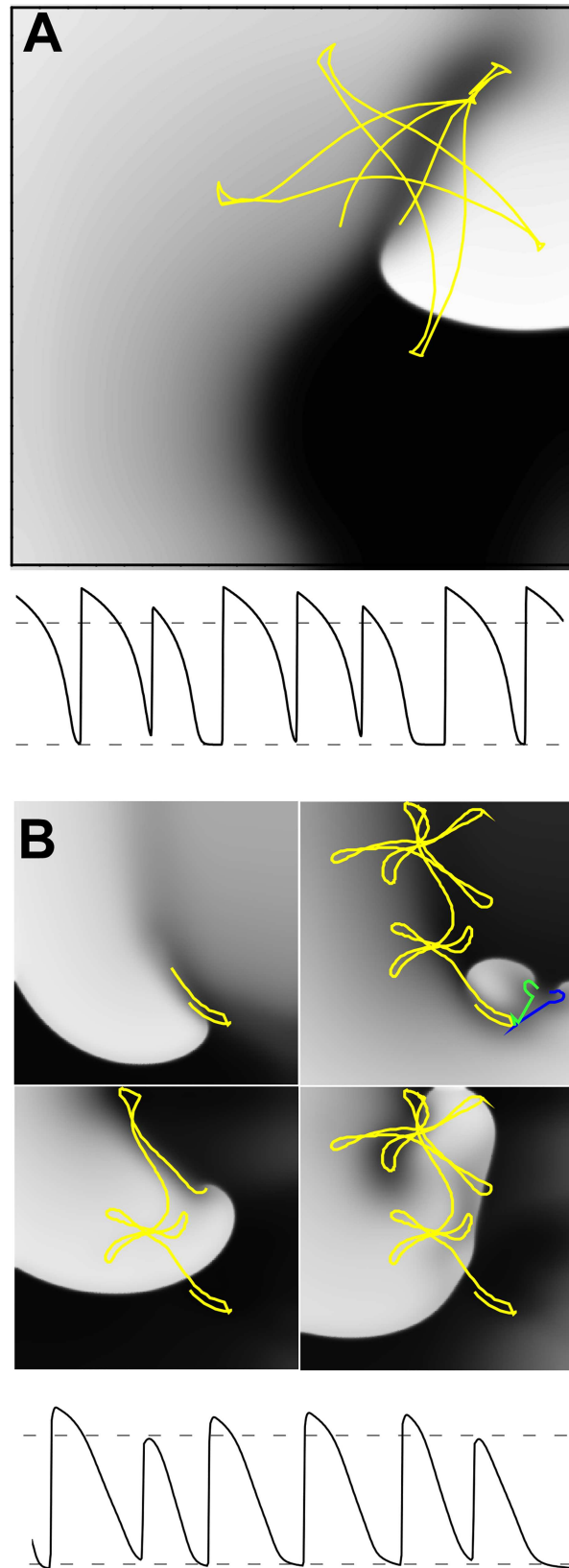
Fig 5. Simulations of functional reentry for PR model (A) and Mahajan model (B). Tip trajectories overlaid in yellow, green, and blue, 5 cm x 5 cm grids and $D = 1$ cm^2/s.

doi:10.1371/journal.pcbi.1005087.g005
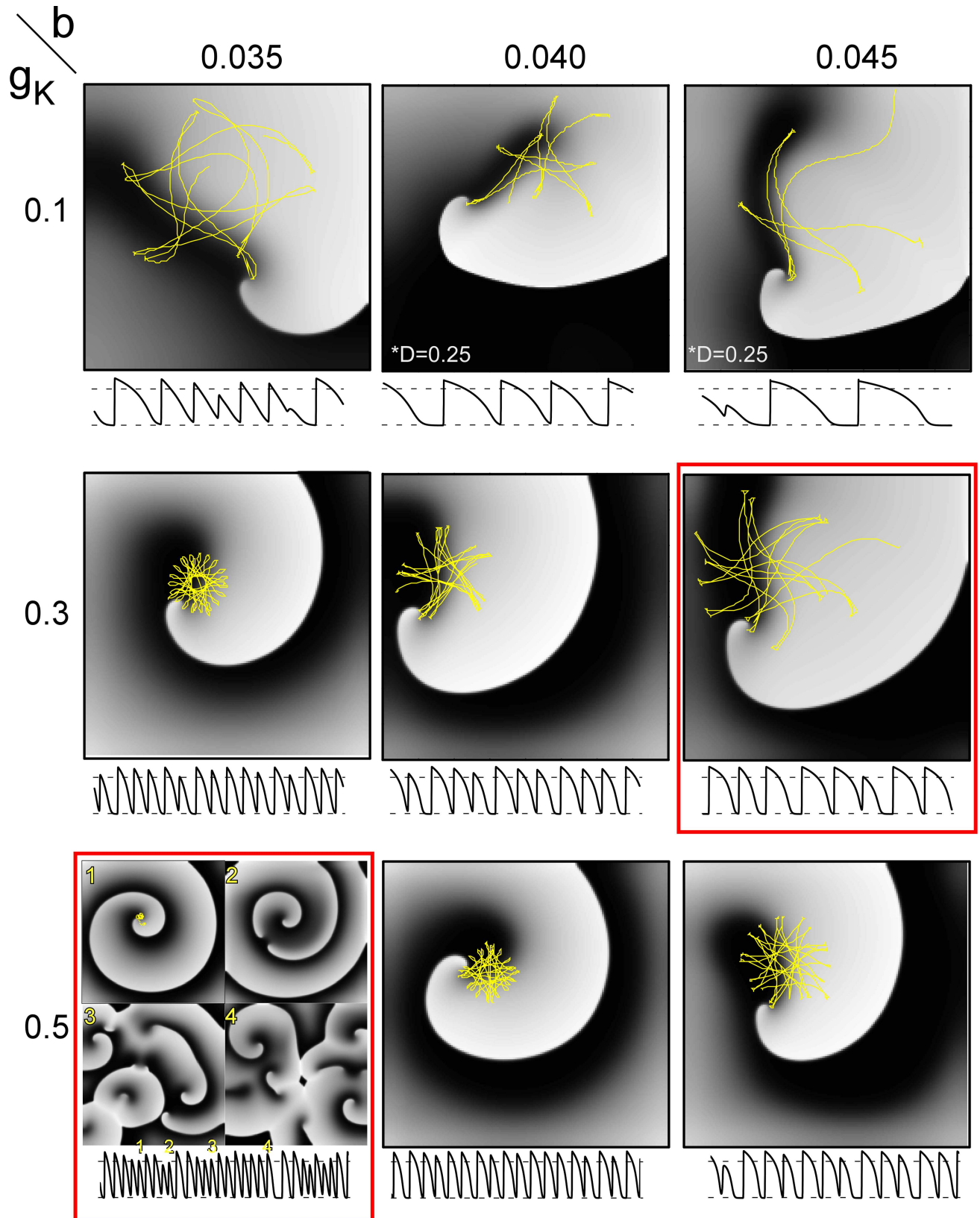
Fig 6. Spiral wave dynamics as a function of repolarization current I_K parameters (g_K and b). Snapshots of spiral wave patterns are shown in grey scale with the tip trajectories overlaid in yellow. Example V_m signal from one site is shown under each panel with the dashed horizontal lines indicating -83 and 0 mV. Simulations (dt = 0.02 ms and dx = 0.01 cm) were carried out on 4.8 cm x 4.8 cm grids and D = 1 cm^2/s with the exception of the top two right panels where D = 0.25 cm^2/s to account for the larger wavelength. Red boxes indicate that the corresponding videos are available online.

doi:10.1371/journal.pcbi.1005087.g006

in our PR model. We paced the PR cell model with a 2 ms stimuli of -20 pA/pF and found that alternans occurred for cycle lengths between 202 and 210 ms, as shown in **Fig 7**, which is within the range (190–240 ms) reported previously for isolated rabbit myocytes.[26]. Since the PR model contains no repolarization kinetics, we hypothesized that *APD* alternans occurred as a result of alternations of peak I_{Na}, which resulted in alternans in $V_m^{\max}$, which caused alternans in *APD*. Since I_{Na} is negligible except during depolarization, *APD* is a function of only $V_m^{\max}$ (and can be computed by integrating **Eq 7** with initial condition $V_m = V_m^{\max}$). Since alternations in the variable *h* were more pronounced than *m* (see **Fig 7B**), we hypothesized that only I_{Na} *in*activation kinetics are necessary for cellular alternans. A "reduced" two variable (V_m,*h*) model, in which variable m^3 was replaced with function $m_\infty^3(V_m)$ and g_{Na} was reduced to 5.8 mS/μF (to maintain $CV = 55cm / s$), confirmed that I_{Na} *in*activation by itself was capable of generating cellular alternans in our PR model.

Discussion

Traditionally, cardiac AP models have been developed from equations and parameters derived from voltage clamp experiments. Many currents have voltage-dependent gating variables whose characterization via voltage clamp provides intuitive and meaningful parameters. However, in order to obtain such parameters it is necessary to isolate individual currents either chemically, functionally, or genetically. In addition, the relationship of voltage-clamp derived parameters to AP characteristics in single cells and during propagation is complex, non-intuitive, and often involves the interaction of multiple variables.

Here we provide an alternative approach in which we calibrate our model in such a way as to reproduce certain AP behavior under physiological conditions *while including all available voltage clamp data*. In this way, our PR model is both physiologically meaningful and parsimonious. It is physiological because it incorporates HH-like equations and parameters with only *one phenomenological* parameter *b* which controls AP shape. It is parsimonious because it was constructed was constructed to reproduce the specific set of experimental data sets (Figs 1–3) that capture important electrophysiological behavior with as few parameters as possible. In addition, we have recently shown that this model is mathematically identifiable (i.e., not over parameterized)[45]. Incidentally, as described by Biktashev et al. [46] FitzHugh–Nagumo models fail to reproduce some features of cardiac ionic models such as: slow repolarization, slow sub-threshold response, non-Tikhonov asymptotic properties of excitability [47], wave front dissipation [48], and different action potential amplitude in single cells versus propagation [9] which our model captures (see Fig 2).

Physiological models are developed using a set of experimental calibration data, which for our model is for rabbit tissue and myocytes at physiological temperature and heart rate. Our approach should be relatively straight-forward to implement for other species, although this will require the high-fidelity measurement of the dynamic I-V curve during propagation [33] and in single cells as well as the recovery of excitability in isolated myocytes [32]. As far as we are aware, our PR model is the first to include dynamic I-V curves during propagation into its development (i.e., calibration) which we believe is superior to simply adjusting g_{Na} to match CV. We believe that proper extensions of our PR model will include additional constraints
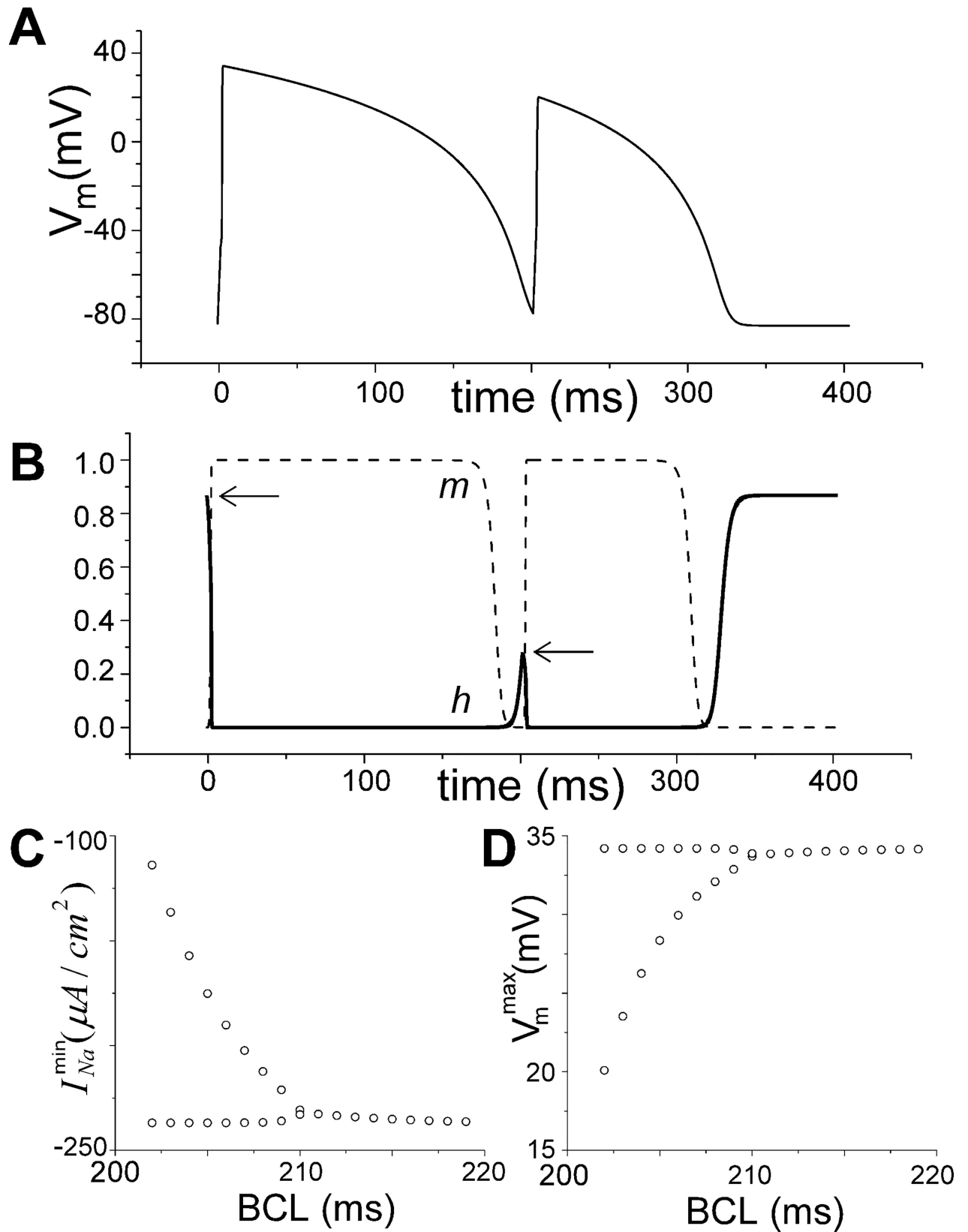
Fig 7. Cellular alternans in PR model during pacing. A) Beat-to-beat dynamics of sequential action potentials during periodic pacing at BCL = 202 ms. B) The corresponding dynamics of the activation m (dashed line) and inactivation h (solid line) variables. Note the similarity of m for subsequent beats while h alternates as shown by arrows. Bifurcation diagrams illustrating steady state alternans in I_{Na}^{min} C) and V_m^{max} D) as a function of BCL.

obtained using appropriate data sets during recalibration. One reason we think our model is useful is because it has only one inward current which is non-zero only during depolarization, and only one outward current. Unlike traditional models in which multiple combinations of currents can give rise to the same AP shape [49], in our model repolarization is characterized only by a time-independent, voltage dependent current (I_K), and therefore, I_K parameters completely determines AP shape [33]. In addition, each current typically incorporates one or two variables (often gates). Despite the non-uniqueness of the relationship between model parameters and AP shape, model developers have largely ignored the interaction of the various currents and variables (components) in simulations. For a model with $n > 1$ components, the total number of possible interactions between two or more components, excluding the full model of all n components, is $2^n - n - 2$. Traditional models have at least 10 components, which results in over 1000 interactions! Characterizing these interactions appropriately both physiologically and mathematically continues to be a significant challenge.

[2, 31, 50, 51]The simplicity of our model allows unique *physiological* insight regarding the interaction of depolarization and repolarization processes. We found that I_K conductance (g_K) is related to the cycle length of reentry (see Fig 6) consistent with the experimental findings of Warren et al. in guinea pig [52]. In addition, our PR model exhibited the expected relationship between *APD* and spiral wave behavior [53]; specifically, the frequency of activity for single spiral was inversely related to *APD*, and also inversely related to the region covered by the spiral wave tip.

Surprisingly, our PR model (comprised of only a HH I_{Na} current with only two gating variables and a time-independent, voltage-dependent I_K current) exhibited important "emergent" behavior including cellular alternans (Fig 7), unstable spiral waves (Figs 5 and 6), and even spiral wave breakup (Fig 6, bottom left panel). We initially thought that alternans and spiral wave breakup would require dynamic repolarization variables with time constants with values close to the *APD* capable of generating *APD* alternans. We only discovered spiral breakup serendipitously while performing a sensitivity analysis of the spiral wave meandering behavior on the I_K repolarization parameters. It is important to note, however, that the parameter set for which breakup occurred ($g_K = 0.5, b = 0.035$) resulted in a rate (~30 Hz) which is twice that observed in experiments.[54, 55]

While our PR model reproduces important physiologically meaningful behavior, it does have limitations. It should be noted that the alternans resulting from the interaction of I_{Na} and I_K are the 'minimal' requirements, other currents such as I_{to} and I_{CaL} may either enhance or suppress this behavior. Our PR model does not include intracellular calcium dynamics, nor the majority of repolarization membrane currents. It should be noted that the Tyrode's solution used to perfuse the hearts from which the propagation I-V experimental data were obtained (Fig 2) in the presence of 15 mM diacetyl monoxime, however the longitudinal propagation velocity was 59 ± 3 cm/s which is within the range reported for the rabbit without any uncoupling agents (see Table B in S1 Text). The I_{Na} equations are of HH type, Markov models are required to replicate certain features of voltage clamp experiments including drug binding kinetics.[50] Importantly, the *APD* in our model is dependent on V_m^{max} which depends on the stimulus current, which is different in single cells compared to in tissue during propagation. When the PR model is stimulated to unphysiologically large V_m the *APD* is unphysiologically long; to avoid this in tissue simulations we initiated propagation in the cable by holding V_m at the end (1 mm) at 0 mV for 2 ms.

One significant difference between our I_{Na} sub-model and previous rabbit I_{Na} sub-models is that we did not include a slow inactivation gate. While slow inactivation of I_{Na} can be justified from voltage clamp experiments [31], we have found that it can induce unphysiological post repolarization refractoriness as shown in Fig 3 and [51]. In addition, the I_{Na} sub-model in the existing rabbit models are the same as LR1 in which the slow inactivation kinetics were derived from sheep and calf trabeculae muscles in which spatial homogeneity of V_m and VC control are lacking. We believe that much more research is needed to appropriately incorporate slow inactivation of I_{Na} (as well as late I_{Na}) into AP models, especially those used to simulate propagation. Incidentally, ten Tusscher et al. interpolated experimental time constants of fast and slow activation as a function of voltage over the range -80 to -40 mV in which data is not available to values more than four times values outside of this range (see Fig 1 D & E in [2]).

Our novel PR model provides unique and physiological generalizable insight into the relationship among gating kinetics and AP behavior in single cells and during propagation. We show unequivocally that only two currents (I_{Na},I_K) and three variables (V_m,m,h) are required to reproduce cellular alternans and spiral wave breakup. In fact, only two variables (V_m,h) are required to produce alternans and implicate a destabilizing effect resulting from the interaction of the non-linear rectification of I_K [56] and the voltage and time dependence of h. We believe that our PR model is an ideal tool to quantify excitability and propagation related to a variety of important physiological and pathophysiological issues. For example our model can be used to study the effects of drugs (our model predicts that an 83% decrease of g_{Na} is required for propagation failure), genetic mutations of SCN5A such as LQT3, and the differences between atrial and ventricular tissue. In addition we believe that it provides a solid "building-block" to develop more realistic rabbit AP models by including additional sub-models (e.g., I_{CaL}, I_{to}, I_{Kr} and intracellular calcium handling).

All experimental data and PR simulation results presented in this paper (with the exception of the videos) will be made available online at Research Gate. The model will be uploaded to CellML.

Supporting Information

S1 Text. Supplementary information including Tables A and B as well as Figs A, B and C. (DOCX)

S1 Video. Spiral wave dynamics $g_K = 0.3 mS / \mu F$ and $b = 0.0.45 mV^{-1}$. (AVI)

S2 Video. Spiral wave dynamics $g_K = 0.5 mS / \mu F$ and $b = 0.0.35 mV^{-1}$. (AVI)

Author Contributions

Conceptualization: RAG.

Formal analysis: RAG PP.

Investigation: RAG.

Methodology: RAG.

Software: RAG.

Validation: RAG PP.

Visualization: RAG.

Writing – original draft: RAG.

Writing – review & editing: RAG PP.

References

1. Hodgkin AL, Huxley AF. A quantitative description of membrane current and its application to conduction and excitation in nerve. J Physiol. 1952; 117(4):500–44. doi: 10.1113/jphysiol.1952.sp004764 PMID: 12991237

2. ten Tusscher KH, Noble D, Noble PJ, Panfilov AV. A model for human ventricular tissue. Am J Physiol Heart Circ Physiol. 2004; 286(4):H1573–H89. doi: 10.1152/ajpheart.00794.2003 [pii]. PMID: 14656705

3. Iyer V, Mazhari R, Winslow RL. A computational model of the human left-ventricular epicardial myocyte. Biophys J. 2004; 87(3):1507–25. doi: 10.1529/biophysj.104.043299 PMID: 15345532; PubMed Central PMCID: PMC1304558.

4. Niederer SA, Fink M, Noble D, Smith NP. A meta-analysis of cardiac electrophysiology computational models. Exp Physiol. 2009; 94(5):486–95. [pii]; doi: 10.1113/expphysiol.2008.044610 PMID: 19139063

5. Fink M, Noble D. Markov models for ion channels: versatility versus identifiability and speed. Philos Trans A Math Phys Eng Sci. 2009; 367(1896):2161–79. 367/1896/2161 [pii]; doi: 10.1098/rsta.2008.0301 PMID: 19414451

6. Surovyatkina E, Noble D, Gavaghan D, Sher A. Multistability property in cardiac ionic models of mammalian and human ventricular cells. Prog Biophys Mol Biol. 2010; 103(1):131–41. doi: 10.1016/j.pbiomolbio.2010.01.004 PMID: 20153355.

7. Zaniboni M. 3D current-voltage-time surfaces unveil critical repolarization differences underlying similar cardiac action potentials: A model study. Math Biosci. 2011; 233(2):98–110. S0025-5564(11)00103-9 [pii]; doi: 10.1016/j.mbs.2011.06.008 PMID: 21781977

8. ten Tusscher KH, Bernus O, Hren R, Panfilov AV. Comparison of electrophysiological models for human ventricular cells and tissues. Prog Biophys Mol Biol. 2006; 90(1–3):326–45. S0079-6107(05)00030-1 [pii]; doi: 10.1016/j.pbiomolbio.2005.05.015 PMID: 16002127

9. Cherry EM, Fenton FH. A tale of two dogs: analyzing two models of canine ventricular electrophysiology. Am J Physiol Heart Circ Physiol. 2007; 292(1):H43–H55. doi: 10.1152/ajpheart.00955.2006 PMID: 16997886

10. Cooper J, Mirams GR, Niederer SA. High-throughput functional curation of cellular electrophysiology models. Prog Biophys Mol Biol. 2011; 107(1):11–20. doi: 10.1016/j.pbiomolbio.2011.06.003 PMID: 21704062.

11. Fink M, Noble PJ, Noble D. Ca(2)(+)-induced delayed afterdepolarizations are triggered by dyadic subspace Ca2(2)(+) affirming that increasing SERCA reduces aftercontractions. Am J Physiol Heart Circ Physiol. 2011; 301(3):H921–35. doi: 10.1152/ajpheart.01055.2010 PMID: 21666112; PubMed Central PMCID: PMC3191104.

12. Ji YC, Gray RA, Fenton FH. Implementation of Contraction to Electrophysiological Ventricular Myocyte Models, and Their Quantitative Characterization via Post-Extrasystolic Potentiation. PLoS One. 2015; 10(8):e0135699. Epub 2015/09/01. doi: 10.1371/journal.pone.0135699 PMID: 26317204; PubMed Central PMCID: PMCPMC4552858.

13. Pathmanathan P, Gray RA. Ensuring reliability of safety-critical clinical applications of computational cardiac models. Front Physiol. 2013; 4:358. Epub 2014/01/01. doi: 10.3389/fphys.2013.00358 PMID: 24376423; PubMed Central PMCID: PMCPMC3858646.

14. Jost N, Papp JG, Varro A. Slow delayed rectifier potassium current (IKs) and the repolarization reserve. Ann Noninvasive Electrocardiol. 2007; 12(1):64–78. doi: 10.1111/j.1542-474X.2007.00140.x PMID: 17286653.

15. Ito H, Glass L. Spiral breakup in a new model of discrete excitable media. Phys Rev Lett. 1991; 66(5):671–4. doi: 10.1103/PhysRevLett.66.671 PMID: 10043869

16. Karma A. Spiral breakup in model equations of action potential propagation in cardiac tissue. Phys Rev Lett. 1993; 71(7):1103–6. doi: 10.1103/PhysRevLett.71.1103 PMID: 10055449

17. Aliev RR, Panfilov AV. Modeling of heart excitation patterns caused by a local inhomogeneity. J Theor Biol. 1996; 181(1):33–40. S0022-5193(96)90112-5 [pii]; doi: 10.1006/jtbi.1996.0112 PMID: 8796189

18. Fenton F, Karma A. Vortex dynamics in three-dimensional continuous myocardium with fiber rotation: Filament instability and fibrillation. Chaos. 1998; 8(1):20–47. doi: 10.1063/1.166311 PMID: 12779708

19. Mitchell CC, Schaeffer DG. A two-current model for the dynamics of cardiac membrane. Bull Math Biol. 2003; 65(5):767–93. [pii]; doi: 10.1016/S0092-8240(03)00041-7 PMID: 12909250

20. Kirkton RD, Bursac N. Engineering biosynthetic excitable tissues from unexcitable cells for electrophysiological and cell therapy studies. Nat Commun. 2011; 2:300. [pii]; doi: 10.1038/ncomms1302 PMID: 21556054

21. Lu Z, Kamiya K, Opthof T, Yasui K, Kodama I. Density and kinetics of I(Kr) and I(Ks) in guinea pig and rabbit ventricular myocytes explain different efficacy of I(Ks) blockade at high heart rate in guinea pig and rabbit: implications for arrhythmogenesis in humans. Circulation. 2001; 104(8):951–6. doi: 10.1161/hc3401.093151 PMID: 11514385.

22. Panfilov AV. Is heart size a factor in ventricular fibrillation? Or how close are rabbit and human hearts? Heart Rhythm. 2006; 3(7):862–4. doi: 10.1016/j.hrthm.2005.12.022 PMID: 16818223

23. Hondeghem LM, Lu HR, van Rossem K, De Clerck F. Detection of proarrhythmia in the female rabbit heart: blinded validation. J Cardiovasc Electrophysiol. 2003; 14(3):287–94. doi: 10.1046/j.1540-8167.2003.02466.x PMID: 12716112.

24. Puglisi JL, Bers DM. LabHEART: an interactive computer model of rabbit ventricular myocyte ion channels and Ca transport. Am J Physiol Cell Physiol. 2001; 281(6):C2049–C60. PMID: 11698264

25. Shannon TR, Wang F, Puglisi J, Weber C, Bers DM. A mathematical treatment of integrated Ca dynamics within the ventricular myocyte. Biophys J. 2004; 87(5):3351–71. doi: 10.1529/biophysj.104.047449 PMID: 15347581

26. Mahajan A, Shiferaw Y, Sato D, Baher A, Olcese R, Xie LH, et al. A rabbit ventricular action potential model replicating cardiac dynamics at rapid heart rates. Biophys J. 2008; 94(2):392–410. S0006-3495(08)70718-5; doi: 10.1529/biophysj.106.98160 PMID: 18160660

27. Aslanidi OV, Sleiman RN, Boyett MR, Hancox JC, Zhang H. Ionic mechanisms for electrical heterogeneity between rabbit Purkinje fiber and ventricular cells. Biophys J. 2010; 98(11):2420–31. doi: 10.1016/j.bpj.2010.02.033 PMID: 20513385; PubMed Central PMCID: PMC2877343.

28. Luo CH, Rudy Y. A model of the ventricular cardiac action potential. Depolarization, repolarization, and their interaction. Circ Res. 1991; 68(6):1501–26. doi: 10.1161/01.res.68.6.1501 PMID: 1709839

29. Ebihara L, Johnson EA. Fast sodium current in cardiac muscle. A quantitative description. Biophys J. 1980; 32(2):779–90. doi: 10.1016/S0006-3495(80)85016-8 PMID: 7260301

30. Gettes LS, Reuter H. Slow Recovery from Inactivation of Inward Currents in Mammalian Myocardial Fibers. J Physiol-London. 1974; 240(3):703–24. doi: 10.1113/jphysiol.1974.sp010630 PMID: WOS:A1974T872100010.

31. Berecki G, Wilders R, de JB, van Ginneken AC, Verkerk AO. Re-evaluation of the action potential upstroke velocity as a measure of the Na+ current in cardiac myocytes at physiological conditions. PLoS ONE. 2010; 5(12):e15772. doi: 10.1371/journal.pone.0015772 PMID: 21217835

32. Joyner RW, Ramza BM, Osaka T, Tan RC. Cellular mechanisms of delayed recovery of excitability in ventricular tissue. Am J Physiol. 1991; 260(1 Pt 2):H225–H33. PMID: 1992802

33. Gray RA, Mashburn DN, Sidorov VY, Wikswo JP. Quantification of transmembrane currents during action potential propagation in the heart. Biophys J. 2013; 104(1):268–78. Epub 2013/01/22. doi: 10.1016/j.bpj.2012.11.007 PMID: 23332079; PubMed Central PMCID: PMCPMC3540262.

34. Beeler GW, Reuter H. Reconstruction of the action potential of ventricular myocardial fibres. J Physiol. 1977; 268(1):177–210. doi: 10.1113/jphysiol.1977.sp011853 PMID: 874889

35. Sigworth FJ. Voltage Gating of Ion Channels. Quarterly Reviews of Biophysics. 1994; 27(1):1–40. doi: 10.1017/s0033583500002894 PMID: WOS:A1994NK67800001.

36. Bezanilla F. The voltage sensor in voltage-dependent ion channels. Physiological Reviews. 2000; 80 (2):555–92. PMID: WOS:000086032300001.

37. Willms AR, Baro DJ, Harris-Warrick RM, Guckenheimer J. An improved parameter estimation method for Hodgkin-Huxley models. J Comput Neurosci. 1999; 6(2):145–68. PMID: 10333160

38. Pathmanathan P, Gray RA. Filament Dynamics during Simulated Ventricular Fibrillation in a High-Resolution Rabbit Heart. Biomed Res Int. 2015; 2015:720575. Epub 2015/11/21. doi: 10.1155/2015/720575 PMID: 26587544; PubMed Central PMCID: PMCPMC4637469.

39. Livshitz L, Rudy Y. Uniqueness and stability of action potential models during rest, pacing, and conduction using problem-solving environment. Biophys J. 2009; 97(5):1265–76. S0006-3495(09)01159-X [pii]; doi: 10.1016/j.bpj.2009.05.062 PMID: 19720014

40. Sperelakis N, Shumaker HK. Phase-plane analysis of cardiac action potentials. J Electrocardiol. 1968; 1(1):31–41. doi: 10.1016/s0022-0736(68)80006-8 PMID: 5699494.

41. Hunter PJ, McNaughton PA, Noble D. Analytical models of propagation in excitable cells. Prog Biophys Mol Biol. 1975; 30(2–3):99–144. doi: 10.1016/0079-6107(76)90007-9 PMID: 792954

42. Walton MK, Fozzard HA. The conducted action potential. Models and comparison to experiments. Biophys J. 1983; 44(1):9–26. doi: 10.1016/S0006-3495(83)84273-8 PMID: 6626682

43. Gray RA, Huelsing DJ, Aguel F, Trayanova NA. Effect of strength and timing of transmembrane current pulses on isolated ventricular myocytes. J Cardiovasc Electrophysiol. 2001; 12(10):1129–37. Epub 2001/11/09. doi: 10.1046/j.1540-8167.2001.01129.x PMID: 11699521.

44. Schalij MJ, Boersma L, Huijberts M, Allessie MA. Anisotropic reentry in a perfused 2-dimensional layer of rabbit ventricular myocardium. Circulation. 2000; 102(21):2650–8. doi: 10.1161/01.cir.102.21.2650 PMID: 11085970

45. Shotwell MS, Gray RA. Estimability Analysis and Optimal Design in Dynamic Multi-scale Models of Cardiac Electrophysiology. Journal of Agricultural, Biological, and Environmental Statistics. 2016; 21 (2):261–76. doi: 10.1007/s13253-016-0244-7 PMID: 27330268

46. Biktashev VN, Suckley R, Elkin YE, Simitev RD. Asymptotic analysis and analytical solutions of a model of cardiac excitation. Bull Math Biol. 2008; 70(2):517–54. doi: 10.1007/s11538-007-9267-0 PMID: 18060462.

47. Biktashev VN, Brindley J, Holden AV, Tsyganov MA. Pursuit-evasion predator-prey waves in two spatial dimensions. Chaos. 2004; 14(4):988–94. doi: 10.1063/1.1793751 PMID: 15568912

48. Aslanidi OV, Bailey A, Biktashev VN, Clayton RH, Holden AV. Enhanced self-termination of re-entrant arrhythmias as a pharmacological strategy for antiarrhythmic action. Chaos. 2002; 12(3):843–51. doi: 10.1063/1.1500496 PMID: 12779612

49. Zaniboni M, Riva I, Cacciani F, Groppi M. How different two almost identical action potentials can be: a model study on cardiac repolarization. Math Biosci. 2010; 228(1):56–70. S0025-5564(10)00139-2 [pii]; doi: 10.1016/j.mbs.2010.08.007 PMID: 20801131

50. Clancy CE, Rudy Y. Linking a genetic defect to its cellular phenotype in a cardiac arrhythmia. Nature. 1999; 400(6744):566–9. doi: 10.1038/23034 PMID: WOS:000081854800056.

51. Franz MR, Gray RA, Karasik P, Moore HJ, Singh SN. Drug-induced post-repolarization refractoriness as an antiarrhythmic principle and its underlying mechanism. Europace. 2014; 16 Suppl 4:iv39–iv45. Epub 2014/11/02. doi: 10.1093/europace/euu274 PMID: 25362169.

52. Warren M, Guha PK, Berenfeld O, Zaitsev A, Anumonwo JM, Dhamoon AS, et al. Blockade of the inward rectifying potassium current terminates ventricular fibrillation in the guinea pig heart. J Cardiovasc Electrophysiol. 2003; 14(6):621–31. doi: 10.1046/j.1540-8167.2003.03006.x PMID: 12875424

53. Krinsky VI, Efimov IR, Jalife J. Vortices with linear cores in excitable media. Proc R Soc Lond A. 1992; 437:645–55. doi: 10.1098/rspa.1992.0084

54. Samie FH, Mandapati R, Gray RA, Watanabe Y, Zuur C, Beaumont J, et al. A mechanism of transition from ventricular fibrillation to tachycardia: effect of calcium channel blockade on the dynamics of rotating waves. Circ Res. 2000; 86(6):684–91. Epub 2000/04/04. doi: 10.1161/01.res.86.6.684 PMID: 10747005.

55. Chorro FJ, Canoves J, Guerrero J, Mainar L, Sanchis J, Such L, et al. Alteration of ventricular fibrillation by flecainide, verapamil, and sotalol: an experimental study. Circulation. 2000; 101(13):1606–15. doi: 10.1161/01.cir.101.13.1606 PMID: 10747356

56. Delmar M, Michaels DC, Jalife J. Slow recovery of excitability and the Wenckebach phenomenon in the single guinea pig ventricular myocyte. Circ Res. 1989; 65(3):761–74. doi: 10.1161/01.res.65.3.761 PMID: 2475274